Unclassified
SECURITY CLASSIFICATION OF THIS PAGE

CUMENTATION PAGE

Form Approved
OMB No. 0704-0188

AD-A232 204

1b RESTRICTIVE MARKINGS

2b DECLASSIFICATION/DOWNGRADING SCHEDULE

3. DISTRIBUTION/AVAILABILITY OF REPORT
Approved for public release; Distribution unlimited

4 PERFORMING ORGANIZATION REPORT NUMBER(S)
PL-TR-91-2018

5 MONITORING ORGANIZATION REPORT NUMBER(S)

6a NAME OF PERFORMING ORGANIZATION
Phillips Laboratory, Geophysics Directorate

6b OFFICE SYMBOL (If applicable)
PHK

7a. NAME OF MONITORING ORGANIZATION

6c ADDRESS (City, State, and ZIP Code)
Hanscom AFB
Massachusetts 01731-5000

7b ADDRESS (City, State, and ZIP Code)

DTIC ELECTE MAR 15 1991 S D G

8a NAME OF FUNDING/SPONSORING ORGANIZATION

8b OFFICE SYMBOL (If applicable)

9 PROCUREMENT INSTRUMENT IDENTIFICATION NUMBER

8c ADDRESS (City, State, and ZIP Code)

10 SOURCE OF FUNDING NUMBERS

PROGRAM ELEMENT NO	PROJECT NO	TASK NO	WORK UNIT ACCESSION NO
61102F	2303	G2	01

11 TITLE (Include Security Classification)
Cross Sections and Product Kinetic Energy Analysis of H_2O^+ -H_2O Collisions at Suprathermal Energies

12 PERSONAL AUTHOR(S)
C. Randal Lishawa*, Rainer A. Dressler, James A. Gardner**, Richard H. Salter, Edmond Murad

13a TYPE OF REPORT	13b TIME COVERED	14 DATE OF REPORT (Year, Month, Day)	15 PAGE COUNT
Reprint	FROM _____ TO _____	1991 January 29	11

16 SUPPLEMENTARY NOTATION *Summer faculty visitor, Permanent address: Department of Physics and Engineering, Utica College of Syracuse University, Utica NY 13502 - Reprinted from J. Chem. Phys. 93 (5) 1 September 1990 - **Geophysics Research Scholar

17 COSATI CODES		
FIELD	GROUP	SUB-GROUP

18 SUBJECT TERMS (Continue on reverse if necessary and identify by block number)
Ion molecule reactions, Ion-neutral collisions, CO_2 Charge Transfer

19 ABSTRACT (Continue on reverse if necessary and identify by block number)

The reaction of H_2O^+ with H_2O is studied using a longitudinal geometry double mass spectrometer in the collision energy range $E_{c.m.} = 0.5$–25 eV. Cross sections are reported for oxonium ion (H_3O^+) production and the symmetric charge exchange. Isotopic substitution is used to discern the product branches, including the separation of the two channels for oxonium ion production: (i) proton transfer to the target molecule; and (ii) atom pickup by the primary ion. The largest branching ratio is observed for the charge exchange channel, where no isotope effect is detected in the investigated energy range. Proton transfer exhibits the second largest branching ratio and accounts for more than 90% of the oxonium ion production throughout the measured energy range. The proton transfer cross section is dependent on isotopic substitution, while the atom pickup channel is too weak to make a distinct statement

(Cont'd)

20 DISTRIBUTION/AVAILABILITY OF ABSTRACT
☐ UNCLASSIFIED/UNLIMITED ☒ SAME AS RPT ☐ DTIC USERS

21 ABSTRACT SECURITY CLASSIFICATION
Unclassified

22a NAME OF RESPONSIBLE INDIVIDUAL
Edmond Murad

22b TELEPHONE (Include Area Code)
(617) 377-3176

22c OFFICE SYMBOL
PHK

DD Form 1473, JUN 86 Previous editions are obsolete.

SECURITY CLASSIFICATION OF THIS PAGE
Unclassified

91 2 19 214

DTIC FILE COPY

Cont of Block 19:

on its isotopic behavior. Product ion energies, determined by time-of-flight measurements, are also reported for each of the three channels. These measurements show that most (> 95%) of the oxonium ions are formed via a direct, spectator stripping type mechanism while a small amount of reaction products exhibit considerable internal excitation. The charge exchange secondary ions are primarily formed at near-thermal energies in the laboratory frame. Small amounts of high laboratory energy product ions are also observed which at least partly originate through the dissociation of excited oxonium ions.

Cross sections and product kinetic energy analysis of H_2O^+–H_2O collisions at suprathermal energies

C. Randal Lishawa,[a] Rainer A. Dressler, James A. Gardner,[b] Richard H. Salter, and Edmond Murad
Geophysics Laboratory, GL/PHK, Hanscom Air Force Base, Massachusetts 01731

(Received 26 March 1990; accepted 18 May 1990)

The reaction of H_2O^+ with H_2O is studied using a longitudinal geometry double mass spectrometer in the collision energy range $E_{c.m.} = 0.5$–25 eV. Cross sections are reported for oxonium ion (H_3O^+) production and the symmetric charge exchange. Isotopic substitution is used to discern the product branches, including the separation of the two channels for oxonium ion production: (i) proton transfer to the target molecule; and (ii) atom pickup by the primary ion. The largest branching ratio is observed for the charge exchange channel, where no isotope effect is detected in the investigated energy range. Proton transfer exhibits the second largest branching ratio and accounts for more than 90% of the oxonium ion production throughout the measured energy range. The proton transfer cross section is dependent on isotopic substitution, while the atom pickup channel is too weak to make a distinct statement on its isotopic behavior. Product ion energies, determined by time-of-flight measurements, are also reported for each of the three channels. These measurements show that most ($>95\%$) of the oxonium ions are formed via a direct, spectator stripping type mechanism while a small amount of reaction products exhibit considerable internal excitation. The charge exchange secondary ions are primarily formed at near-thermal energies in the laboratory frame. Small amounts of high laboratory energy product ions are also observed which at least partly originate through the dissociation of excited oxonium ions.

I. INTRODUCTION

The bimolecular ion–molecule reaction

$$H_2O^+ + H_2O \rightarrow H_3O^+ + OH \qquad (1)$$

has been the subject of many investigations beginning in 1940.[1] Most of this work has been aimed at measuring the thermal rate coefficient for reaction (1).[2-6] These measurements have agreed on $k_1 \approx 1.9\times10^{-9}$ cm^3 mol^{-1} s^{-1}.

The recent observations of oxonium ions (H_3O^+) in the space shuttle environment[7-9] and in the tails of the comets Giacobini–Zinner[10] and Halley[11] have revived the interest in reaction (1), particularly at suprathermal collision energies. Modeling of the production of the observed H_3O^+ ion densities in the shuttle environment has been particularly difficult due to the lack of information regarding the energy dependence of k_1.[12]

Experiments have been performed at higher collision energies by Turner and Rutherford[13] and by Ryan[14] using a tandem mass spectrometer and a single source high pressure mass spectrometer, respectively. Neither of these studies investigated the symmetric charge exchange or the dynamics of reaction (1).

Reaction (1) can proceed via two direct channels: (i) *atom pickup* in which the primary ion abstracts a hydrogen atom from the target; and (ii) *proton transfer* in which the primary ion transfers a proton to the target molecule. The ionic products of atom pickup are expected to have markedly different laboratory kinetic energies than those of proton transfer. An experiment with product kinetic energy dependent collection efficiency, such as that of Ref. 13, will therefore not determine a correct integral cross section unless mass analysis can separate these two channels and the product collection efficiencies for the two processes are known.

In this paper we present a dynamical study of H_2O^+–H_2O reactions at center-of-mass collision energies in the range 0.5–25 eV. Cross sections and product ion time-of-flight (TOF) measurements are reported for reaction (1) and the symmetric charge exchange. The two channels of reaction (1) are separated by studying the atom pickup reactions:

$$H_2{}^{18}O^+ + D_2O \rightarrow H_2D{}^{18}O^+ + OD, \qquad (2a)$$

$$D_2{}^{18}O^+ + H_2O \rightarrow HD_2{}^{18}O^+ + OH, \qquad (2b)$$

and the proton (deuteron) transfer reactions:

$$H_2O^+ + D_2{}^{18}O \rightarrow OH + HD_2{}^{18}O^+, \qquad (3a)$$

$$D_2O^+ + D_2{}^{18}O \rightarrow OD + D_3{}^{18}O^+. \qquad (3b)$$

Charge exchange collision cross sections are obtained from the isotopic reactions:

$$H_2O^+ + D_2{}^{18}O \rightarrow H_2O + D_2{}^{18}O^+, \qquad (4a)$$

$$D_2{}^{18}O^+ + H_2O \rightarrow D_2{}^{18}O + H_2O^+. \qquad (4b)$$

In addition, the ionic product OH^+ is observed, which we associated with the collision-induced dissociation channel:

$$H_2O^+ + H_2O \rightarrow OH^+ + H + H_2O. \qquad (5)$$

This channel is investigated using reaction (5a):

$$D_2O^+ + H_2{}^{18}O \rightarrow OD^+ + D + H_2{}^{18}O. \qquad (5a)$$

[a] Summer faculty visitor, 1989. Permanent address: Department of Physics and Engineering, Utica College of Syracuse University, Utica, NY 13502.
[b] Geophysics Research Scholar.

 0021-9606/90/173196-11$03.00

II. EXPERIMENTAL

The apparatus used in the present work is a longitudinal geometry double mass spectrometer. The instrument and the measurement procedures have been described in detail previously.[16-18] The primary water ion beam is formed in an electron impact ion source at ionizing electron energies between 20 and 30 eV. The ions are accelerated to a potential of 150 V and passed through a Wien Filter (Colutron Research) to produce a mass selected primary beam. The desired ion energy is obtained with two deceleration lenses. The primary beam traverses a 0.27 cm long, gold plated collision cell with mesh-covered apertures. The target water vapor pressure in the collision cell is approximately 1.33 Pa (10^{-3} Torr), which is measured with a capacitance manometer (MKS Baratron 390H). The primary and product ions exiting the collision chamber are accelerated and focused by a series of grids into a quadrupole mass filter (Extranuclear). Ions selected by the mass filter are detected with a channel electron multiplier (Galileo Electro-Optics).

The primary ion energy is determined by ramping a retardation potential on one of the focusing grids following the collision chamber. The derivative of the obtained retardation curve exhibits a minimum at which the ion beam energy is defined. These energies are confirmed by measuring the times of flight of primary beam pulses.

It has been shown in previous work[17,18] that, due to the limited collection angle of the collision chamber geometry, knowledge of the product ion angular distribution is necessary in order to determine integral cross sections. The required information on the angular distribution can frequently be obtained through analysis of the TOF spectra. In the case of isotropically scattered product ions in the laboratory frame (normally thermal ions), the average solid collection angle determines the fraction of ions that exit the collision chamber. We have calculated the average solid collection angle of the present collision chamber geometry, from which we determine a collection efficiency for isotropically scattered ions to be 20.8%, provided all ions exiting the collision chamber are detected.

When measuring cross sections, a high acceleration potential of 80 V is applied between the collision chamber and the quadrupole entrance. This results in close to 100% collection of ions exiting the collision chamber. During TOF measurements, the acceleration potential is reduced to 20 V to improve the TOF resolution. This, however, significantly reduces the collection efficiency of slow ions which leave the collision chamber at large angles with respect to the primary beam axis. We have measured the collection efficiency of thermal ions in the TOF mode to be, by a factor of 6, lower than in the cross section mode.

Since there is no detectable attenuation of the primary beam, the experimental (raw) cross sections are calculated from

$$\sigma_{\text{exp}} = I_{\text{sec}}/I_{\text{prim}}nl, \tag{6}$$

where I_{sec} and I_{prim} are the intensities of the secondary and primary beams, respectively, n is the target gas density, and l is the effective interaction length.

The TOF spectra are obtained by pulsing the ion beam prior to the collision chamber with a pulsing electrode and by measuring the arrival time of the ions at the detector. The pulse width of the primary ions is set between 0.5 and 1.5 μs. The laboratory energies of the product ions are calculated using basic electrostatic equations and the measured primary ion times of flight.

We find little to no dependence of the measured cross sections on electron energy, indicating a negligible presence of metastable ions. Nevertheless, an uncertainty exists regarding the internal state distribution of the primary ion beam. Lindemann *et al.*[19] have studied the abundance of electronic states of H_2O^+ produced by electron ionization of H_2O, finding approximately 45% of the ions in the $\tilde{X}\,^2B_1$ and 45% in the $\tilde{A}\,^2A_1$ state at an electron energy of 30 eV. The Franck–Condon factors[20,21] for ionization into the $\tilde{A}$ state indicate that these ions are produced in vibrationally excited levels of the ν_2 bending mode. These levels are known to have radiative lifetimes around 800 ns.[22] The flight time of the ions from the source to the collision chamber is longer than 10 μs. We therefore conclude that the amount of primary ions in the $\tilde{A}$ excited state is negligible. We cannot exclude the possibility of vibrationally excited primary ions. The Franck–Condon factors for vibrational excitation in the ground ionic state are, however, relatively small, and the emission spectrum of $\tilde{A}$ state water ions produced through electron impact is dominated by $(0,\nu_2',0)$–$(0,0,0)$ transitions,[23,24] indicating that the primary ions are essentially in low vibrational levels.

The water isotopes were obtained from Cambridge Isotope Labs with initial purities D_2O (99.7% D), $D_2{}^{18}O$ (98% D, 98% ^{18}O), and $H_2{}^{18}O$ (98% ^{18}O). The target water isotopic purity is checked by measuring the product isotope abundances observed in the charge exchange reaction of N_2^+ with the water sample.[17] The correct partial pressure of the target gas is then obtained from the measured abundance of the investigated isotope.

III. RESULTS

A. Atom pickup channel

The atom pickup channel measurements are obtained from reactions (2a) and (2b). Reaction (2a) is used for the TOF measurements, while cross sections for hydrogen atom and deuterium atom pickup are obtained from both reactions. TOF measurements of the hydrogen atom pickup reaction (2b) are difficult to analyze since they suffer from large contributions of the primary ion current, which in this case is poorly discriminated in the quadrupole mass filter.

The TOF spectra obtained for reaction (2a) at a primary ion laboratory energy of 29.5 eV are shown in Fig. 1. The lower curve is the primary beam TOF spectrum and the upper curve is the TOF spectrum of ionic products of mass 20. A TOF-to-product-laboratory-energy converted scale is included in the figure. The laboratory energies are calculated assuming the products are produced near the collision chamber exit and with a scattering angle of 0°. The product ions are observed in a narrow band at a time of flight corresponding to 23.7 ± 2.3 eV.

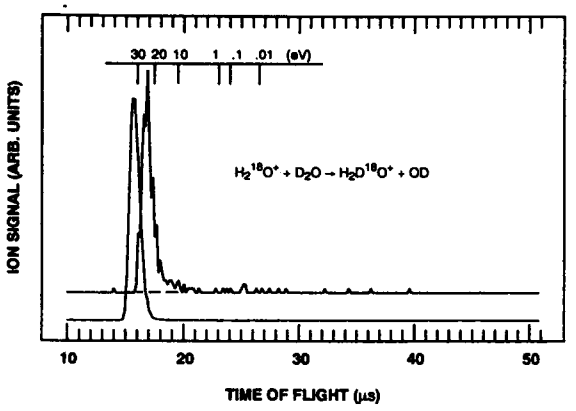

FIG. 1. TOF spectrum of $H_2D^{18}O^+$ (upper curve) produced through atom pickup by $H_2{}^{18}O^+$ from D_2O at a laboratory ion energy of 29.5 eV ($E_{c.m.}$ = 14.8 eV). The lower curve is the TOF spectrum of the primary ion $H_2{}^{18}O^+$. The inserted scale represents the converted product laboratory energies.

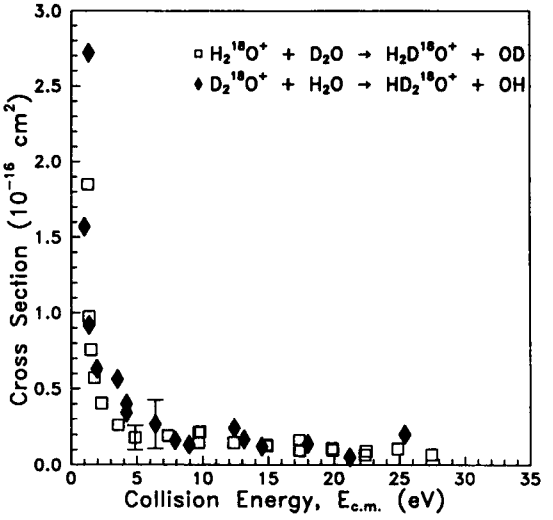

FIG. 2. Collision energy dependence of the cross section for the atom pickup reactions (2a) and (2b).

The TOF spectra of reaction (2a) have the same characteristics throughout the measured energy range. Table I lists the product laboratory energies for reaction (2a). The product ions have considerable forward energy in the laboratory frame. Since these bands are also narrow throughout the measured energy range, we conclude that most of the ions are scattered at very small laboratory angles and that the product ions are therefore collected efficiently. The measured raw cross sections are consequently a good representation of the integral cross sections.

The energy dependence of the measured cross sections for reactions (2a) and (2b) is plotted in Fig. 2. The small difference in mass between the primary and secondary ions in reaction (2b) necessitates the subtraction of a normalized background spectrum obtained without a target gas from the mass spectrum obtained with the target sample. The error in the data is consequently larger for reaction (2b). Examples of error bars are shown in the figure. The large relative errors do not permit the identification of an isotope dependence of the atom pickup cross section.

B. Proton transfer channel

The proton (deuteron) transfer measurements are performed on reactions (3a) and (3b). The TOF spectra shown in Fig. 3 were obtained from reaction (3a) at a primary ion energy of 29.3 eV, corresponding to a center-of-mass collision energy of 16.1 eV. Both the primary ion and product ion TOF spectra are shown. The product ions exhibit two main bands at this energy: one at near-thermal energy (first band) and one at higher laboratory energy (second band.)[25] The arrow shown in Fig. 3 indicates 7.5 eV, which is the laboratory energy expected in the case of zero-kinetic-energy release in the center-of-mass frame, assuming a stationary target. This energy corresponds to the translational energy of product ions moving at the center-of-mass velocity $v_{c.m.}$

$$E_{sec}(E_{kin}=0) = (m_3/2)\cdot v_{c.m.}^2, \quad (7)$$

where m_3 is the secondary ion mass. Transforming in terms of the laboratory primary ion energy E_{prim}, one obtains

$$E_{sec}(E_{kin}=0) = [m_3 m_1/(m_1+m_2)^2 \cdot E_{prim}], \quad (8)$$

TABLE I. Ion product laboratory energies E_{sec} from TOF measurements of the atom pickup reaction (2a). E_{prim} is the laboratory primary ion energy and $E_{c.m.}$ is the center-of-mass collision energy.

$H_2{}^{18}O^+ + D_2O \rightarrow H_2D^{18}O^+ + OD$ (2a)		
E_{prim} (eV)	$E_{c.m.}$ (eV)	E_{sec} (eV)
4.3	2.15	2.7 ± 1.2
9.3	4.65	7.1 ± 1.5
13.9	6.95	10.3 ± 1.7
19.5	9.75	13.8 ± 2.2
29.5	14.8	23.7 ± 2.3
39.5	19.8	32.9 ± 3.0

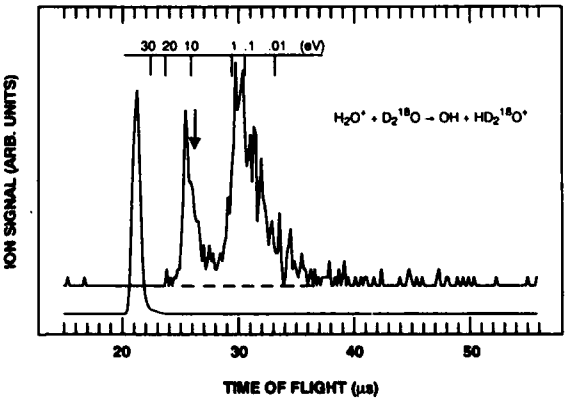

FIG. 3. TOF spectrum of $HD_2{}^{18}O^+$ (upper curve) produced through proton transfer from H_2O^+ to $D_2{}^{18}O$ at a laboratory ion energy of 29.3 eV ($E_{c.m.}$ = 15.9 eV). The lower curve is the TOF spectrum of the primary ions. The inserted scale represents the converted product laboratory energies. The arrow in the figure indicates the laboratory energy corresponding to zero-kinetic-energy release in the center-of-mass frame.

where m_1 is the primary ion mass and m_2 is the neutral target mass.

Since the most intense band is located at lower laboratory velocities than the center-of-mass velocity, we consider the band to be due to ions which are scattered backward in the center-of-mass frame. The peak of the second band occurs close to the center-of-mass velocity, indicating the production of ions which are either scattered at large angles or which are forward scattered in the laboratory frame with little center-of-mass kinetic energy. The narrow width of the band indicates that the ions are scattered within a narrow range of laboratory angles, therefore suggesting that these ions are produced with little center-of-mass kinetic energy.

The TOF spectra shown in Fig. 4 were obtained from reaction (3b) at a primary ion energy of 29.1 eV ($E_{c.m.} = 15.2$ eV). In this isotopic reaction, two main bands are also observed, the more intense band of which is at near-thermal energies. The peak of the higher energy band (second band) occurs at the energy indicated by the arrow for zero-kinetic-energy release in the center-of-mass frame. An additional very weak band (third band) is observed which is centered at a laboratory energy of 22.7 eV. This band is also detected in some spectra of reaction (3a), but is generally less intense there. Since these ions have higher laboratory velocities than the center-of-mass velocity, we consider them to be forward scattered in the center-of-mass frame.

As mentioned in the experimental section, the collection efficiency of thermal ions is approximately a factor of 6 lower in the TOF mode than in the cross-section measurement mode. The TOF experiment is therefore considerably more sensitive to high laboratory energy forward peaked ions, since these are collected with nearly equal efficiency in both modes.

Table II lists the measured product laboratory energies

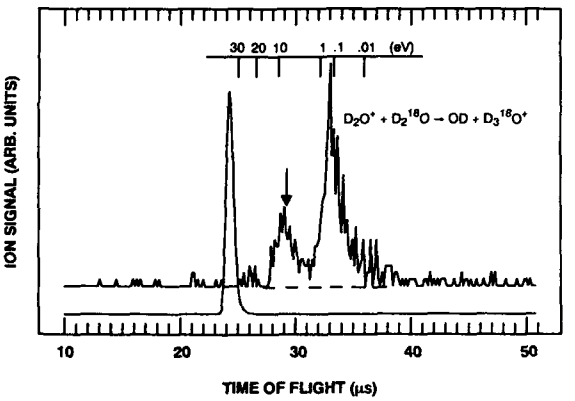

FIG. 4. TOF spectrum of $D_3{}^{18}O^+$ (upper curve) produced through deuteron transfer from D_2O^+ to $D_2{}^{18}O$ at a laboratory ion energy of 29.1 eV ($E_{c.m.} = 15.2$ eV). The lower curve is the TOF spectrum of the primary ions. The inserted scale represents the converted product laboratory energies. The arrow in the figure indicates the laboratory energy corresponding to zero-kinetic-energy release in the center-of-mass frame.

for reations (3a) and (3b) obtained from the TOF band centers. The band centers are obtained from the peaks of computer smoothed bands. Where more than one band is observed, the normalized weight is included in parentheses. The weight of the first band has been multiplied by 6 to correct for the poor extraction efficiency during the TOF measurements. At collision energies below 12 eV, the second band becomes weaker and increasingly less resolved. The indicated weights in poorly resolved cases are only estimates. Table II also includes the laboratory energies corresponding to zero-kinetic-energy release in the center-of-mass frame, calculated using Eq. (8).

TABLE II. Laboratory energies E_{sec} of proton transfer reaction products for reactions (3a) and (3b). E_{prim} is the laboratory primary ion energy, $E_{c.m.}$ is the center-of-mass collision energy, and E_{sec} ($E_{kin} = 0$) is the laboratory energy calculated for zero-kinetic-energy release in the center-of-mass frame.

E_{prim} (eV)	$E_{c.m.}$ (eV)	E_{sec} 1st band (eV)	E_{sec} 2nd band (eV)	E_{sec} 3rd band (eV)	E_{sec} ($E_{kin} = 0$) calc (eV)
$H_2O^+ + D_2{}^{18}O \rightarrow OH + HD_2{}^{18}O^+$ (3a)					
5.1	2.8	0.04 ± 0.05 (1.00)	···	···	1.3
9.5	5.2	0.06 ± 0.07 (0.99)	···	6.4 ± 1.2 (0.01)	2.5
14.3	7.9	0.13 ± 0.07 (0.99)	···	8.1 ± 1.8 (0.01)	3.7
19.0	10.5	0.10 ± 0.05 (0.97)	3.3 ± 1.2 (0.03)	14.4 ± 2.5 (<0.01)	4.9
29.1	16.1	0.11 ± 0.05 (0.97)	10.0 ± 1.8 (0.03)	···	7.5
36.4	20.0	0.07 ± 0.07 (0.89)	12.8 ± 2.0 (0.10)	32.0 ± 3.0 (0.01)	9.4
43.8	24.1	0.15 ± 0.07 (0.86)	14.6 ± 2.3 (0.14)	···	11.3
$D_2O^+ + D_2{}^{18}O \rightarrow OD + D_3{}^{18}O^+$ (3b)					
2.5	1.3	0.23 ± 0.10 (1.00)	···	···	0.7
4.1	2.1	0.07 ± 0.07 (1.00)	···	···	1.1
9.0	4.7	0.12 ± 0.05 (0.98)	···	6.7 ± 1.3 (0.02)	2.5
14.0	7.3	0.13 ± 0.07 (0.99)	···	9.5 ± 1.3 (0.01)	3.8
19.2	10.1	0.18 ± 0.08 (0.98)	5.5 ± 1.2 (0.01)	16.1 ± 1.8 (0.01)	5.2
24.1	12.6	0.19 ± 0.10 (0.95)	6.2 ± 1.2 (0.04)	18.2 ± 2.2 (0.01)	6.6
29.1	15.2	0.21 ± 0.10 (0.94)	8.6 ± 1.5 (0.05)	22.7 ± 2.3 (0.01)	7.9
34.1	17.9	0.09 ± 0.15 (0.95)	9.3 ± 1.5 (0.05)	···	9.3
39.4	20.6	0.17 ± 0.15 (0.81)	15.1 ± 2.0 (0.19)	···	10.7

The second band energies of the proton transfer reaction lie close to, but in most cases slightly above, the zero-kinetic-energy release energies. In the deuteron transfer reaction, there appears to be almost perfect agreement between the second band energies and the zero-kinetic-energy release energies. The data also shows that the near-thermal deuteron transfer product ions are produced at slightly higher laboratory energies than their proton transfer counterparts.

The first band has a statistical weight which is much greater than those of the second and third bands, and therefore the collection efficiency factor for isotropically scattered ions can be applied to obtain the integral proton (deuteron) transfer cross sections. The corrected cross sections for reactions (3a) and (3b) are shown in Fig. 5. An isotope effect is clearly observed: at collision energies above 4 eV, the proton transfer reaction [reaction (3a)] exhibits larger cross sections. The trend is reversed at energies below approximately 4 eV. The proton transfer reaction cross sections are about a factor of 20 times larger that those of the atom-pickup channel. Proton transfer therefore dominates the production of oxonium ions.

C. Charge exchange channel

The symmetric charge exchange channel is studied using reactions (4a) and (4b). The TOF spectra shown in Fig. 6 are from reaction (4b) at $E_{c.m.} = 8.64$ eV. The lower curve is the TOF spectrum for the primary ion mass; the upper curve is the TOF spectrum for the products of mass 18 amu. Two mass 18 peaks are observed, the more intense of which (first band) is produced at near-thermal energy throughout the measured collision energy range. The high energy peak (second band) is also observed in reaction (4a), indicating that this second band cannot be ascribed to products involving a target gas isotopic impurity.

Table III lists the measured laboratory energies of the

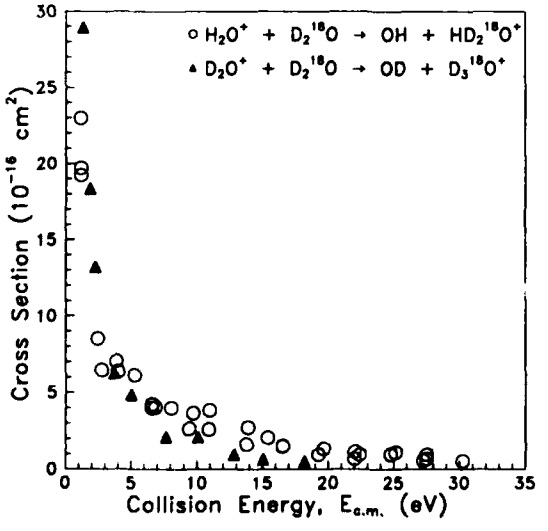

FIG. 5. Collision energy dependence of the cross section for the proton (deuteron) transfer reactions (3a) and (3b). The cross sections have been corrected with respect to a 20.8% collection efficiency.

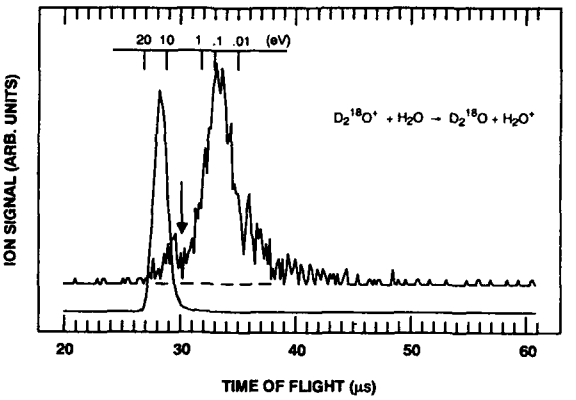

FIG. 6. TOF spectrum of H_2O^+ (upper curve) produced through charge exchange with $D_2{}^{18}O^+$ at collision energy of 8.64 eV (c.m.). The lower curve is the TOF spectrum of the primary ions. The inserted scale represents the converted laboratory energies. The arrow in the figure indicates the laboratory energy corresponding to zero-kinetic-energy release in the center-of-mass frame.

charge exchange products in reactions (4a) and (4b). The normalized weights of the bands are indicated in parentheses. At collision energies below 10 eV, no energies can be determined for the second bands of reaction (4a), since they are poorly resolved. The TOF spectra at lower collision energies, however, clearly exhibit a shoulder adjacent to the near-thermal energy band. In reaction (4b) the second band is adequately resolved as low as $E_{c.m.} = 4$ eV.

The arrow in Fig. 6 indicates the product laboratory energy corresponding to zero-kinetic-energy release. As observed in the deuteron transfer case, the position of the arrow lies near the peak of the second band at this collision energy. The zero-kinetic-energy product ion energies, calculated using Eq. (8), are shown for all of the collision energies in Table III.

Since the main fraction of the signal is formed with near-thermal energy in the laboratory frame, we may assume that the product ions are to a large extent scattered isotropically. The raw cross section data can therefore be corrected with respect to the 20.8% collection efficiency of the instrument. Figure 7 shows the corrected charge exchange integral cross sections for reactions (4a) and (4b). No isotope effect is observed. From the magnitude of the cross section it is seen that charge exchange is the dominant channel of H_2O^+–H_2O reactions at collision energies above 1 eV.

D. OH^+ production

The collision partners of reaction (4b) could not be used for the deuteron transfer study due to the detection of a fast collision product with mass 20 amu which we associated with the collision-induced dissociation of the primary ion, yielding $^{18}OD^+$. The observation of mass 18 ions in reaction (5a) confirms this assumption. In Fig. 8, the TOF spectra are shown which were obtained from reaction (5a) at a collision energy of 14.6 eV. An intense band at high laboratory energies which essentially mimics the primary ion beam is observed as well as an additional band at near-thermal ener-

TABLE III. Laboratory energies E_{sec} of product ion TOF band centers obtained from TOF measurements of the charge exchange reactions (4a) and (4b). E_{prim} is the laboratory primary ion energy, $E_{c.m.}$ is the center-of-mass collision energy, and E_{sec} ($E_{kin} = 0$) is the laboratory energy calculated for zero-kinetic-energy release in the center-of-mass frame.

E_{prim} (eV)	$E_{c.m.}$ (eV)	E_{sec} (eV) 1st band	E_{sec} (eV) 2nd band	E_{sec} ($E_{kin} = 0$) calc
$H_2O^+ + D_2{}^{18}O \rightarrow H_2O + D_2{}^{18}O^+$ (4a)				
5.1	2.81	0.03 ± 0.05	···	1.3
11.0	6.05	0.03 ± 0.05	···	2.7
19.3	10.6	0.16 ± 0.08 (0.90)	4.9 ± 1.2 (0.10)	4.8
29.2	16.1	0.03 ± 0.05 (0.95)	11.8 ± 1.5 (0.05)	7.2
39.6	21.8	0.05 ± 0.05 (0.96)	18.0 ± 2.2 (0.04)	9.8
49.2	27.1	0.05 ± 0.05 (0.95)	21.0 ± 2.2 (0.05)	12.2
$D_2{}^{18}O^+ + H_2O \rightarrow D_2{}^{18}O + H_2O^+$ (4b)				
8.8	3.96	0.06 ± 0.05 (0.99)	5.0 ± 1.2 (0.01)	2.2
19.2	8.64	0.05 ± 0.05 (0.98)	7.8 ± 1.3 (0.02)	4.8
28.3	12.7	0.07 ± 0.08 (0.97)	9.9 ± 1.5 (0.03)	7.0
38.3	17.1	0.06 ± 0.05 (0.98)	16.4 ± 2.0 (0.02)	9.4
48.3	21.7	0.06 ± 0.05 (0.93)	21.8 ± 2.2 (0.07)	9.8

gies. In the absence of a target gas, no mass 18 ions are observed and the band is therefore not due to poor discrimination of the primary beam in the Wien filter or the quadrupole mass filter. The thermal ions are attributable to charge exchange with H_2O impurities in the target gas.

The energy conversion and the narrowness of the high energy band indicate that the OD^+ ions are strongly forward peaked. The primary and product ions are consequently detected with equal efficiency. The energy dependence of the observed reaction cross section is plotted in Fig. 9. Table IV lists the measured laboratory energies of the product ions obtained from TOF measurements.

IV. DISCUSSION

A. H_3O^+ channel

At collision energies above 1–2 eV, reactions in which a light particle is transferred from a donor to an acceptor, such as reaction (1), generally proceed via a spectator stripping type mechanism.[26–31] According to this model the collision can be regarded as solely involving the transferred particle and the acceptor particle. The laboratory velocity of the ionic collision product is then given by the center-of-mass velocity of the transferred and the acceptor particles. The donor particle is considered to be a spectator of the reaction and its velocity remains unchanged throughout the reaction. In Refs. 26–31 this model has been postulated from atom pickup reactions, but there is no reason why the model cannot apply to ion transfer. In the case of atom pickup by an ion

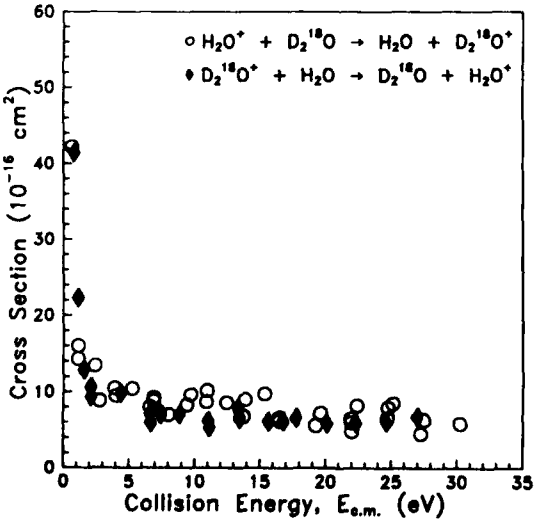

FIG. 7. Collision energy dependence of the charge transfer cross section for reactions (4a) and (4b). The cross sections have been corrected with respect to a 20.8% collection efficiency.

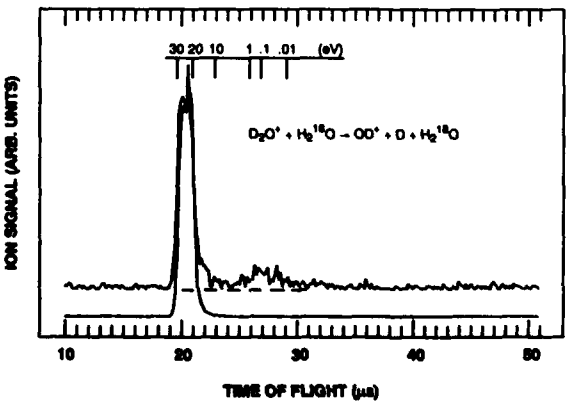

FIG. 8. TOF spectrum of the collision-induced dissociation product OD^+ (upper curve) from D_2O^+–$H_2{}^{18}O$ collisions. Also shown is the primary ion TOF spectrum (lower curve). The inserted scale represents the converted product laboratory energies.

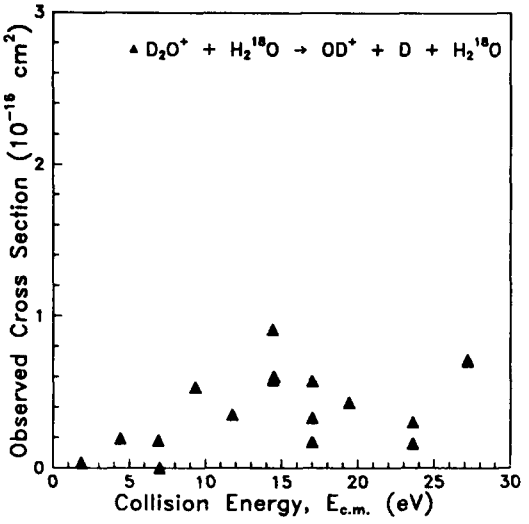

FIG. 9. Collision energy dependence of the cross section for the collision-induced dissociation reaction (5a).

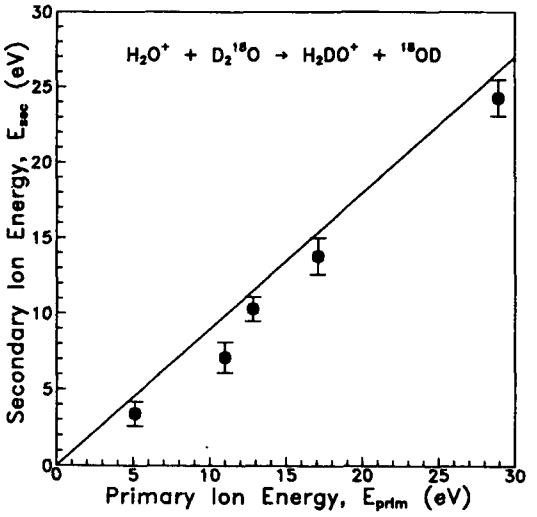

FIG. 10. Ion energy dependence of the laboratory kinetic energy of the H_2DO^+ formed by atom pickup between H_2O^+ and $D_2{}^{18}O$. The dashed line shows the secondary ion energy predicted by the spectator stripping model.

[e.g., reactions (2a) and (2b)], and assuming a stationary target, the laboratory energy of the product ion E_{sec} is given by[17]

$$E_{sec} = (m_1/m_3)\cdot E_{prim}. \quad (9)$$

The model has made accurate predictions of product energies in case of atom pickup reactions such as[26,29]

$$N_2^+ + H_2 \rightarrow N_2H^+ + H. \quad (10)$$

The high laboratory energies of the products in reaction (2a) as well as the narrow bands indicate that the model may also apply to this reaction. Product ion laboratory energies for reaction (2a), determined from the measured times of flight, are plotted in Fig. 10 as a function of the respective primary ion energy. The straight line represents the stripping model ion energy predicted by Eq. (9). The measured energies are seen to lie close to, but consistently below, the predicted energies.

This trend of product velocities being lower than predicted by the model is also observed in the reaction[17]

$$N_2^+ + H_2O \rightarrow N_2H^+ + OH. \quad (11)$$

In that case, the deviation from the model is proposed to be due to a strong short-range bonding interaction resulting in increased momentum transfer. There is no doubt that a strong chemical interaction exists between water ions and water molecules. Tomoda and Kimura[32] have calculated the potential well associated with the water dimer cation to lie approximately 3 eV below the reactant potential. The observed trend therefore further supports the concept of increased momentum transfer due to strong short-range forces. However, a short-range interaction is expected to produce scattering at large angles. This is in contradiction to the observed TOF spectra, which exhibit only little evidence of large-angle scattering. Large-angle scattered products are, however, more prominent in the atom-pickup channel of reaction (11).[17]

The validity of the spectator stripping model could be further checked by examining the isotopic dependence of the measured cross sections. Unfortunately, the very small atom pickup cross sections do not permit a reasonable comparison.

Within the framework of the spectator stripping model, the proton (deuteron) transfer reactions (3a) and (3b) can be considered to proceed solely between the proton (deuteron) and the water target. The product ion is then the association product of the two reactants, and the product laboratory velocity corresponds to the center-of-mass velocity of these two particles. The laboratory product ion velocity v_{sec} is then given by

$$v_{sec} = (m_T/m_3)\cdot v_{prim}, \quad (12)$$

where m_T is the mass of the transferred ion and v_{prim} is the laboratory primary ion velocity. Rearranging to energies yields:

$$E_{sec} = (m_T^2/m_3 m_1)\cdot E_{prim}. \quad (13)$$

TABLE IV. Laboratory energies E_{sec} of collision-induced dissociation ionic products for reaction (5a) obtained from TOF measurements. E_{prim} is the laboratory primary ion energy and $E_{c.m.}$ is the center-of-mass collision energy.

$D_2O^+ + H_2{}^{18}O \rightarrow OD^+ + D + H_2{}^{18}O$ (5a)		
E_{prim} (eV)	$E_{c.m.}$ (eV)	E_{sec} (eV)
3.60	1.80	3.0 ± 1.5
8.30	4.15	6.3 ± 1.2
10.8	5.40	8.0 ± 1.2
13.2	6.60	8.9 ± 1.3
16.6	8.30	13.2 ± 1.8
18.4	9.20	13.9 ± 1.8
20.8	10.4	15.9 ± 2.3
29.2	14.6	24.5 ± 2.3

Equation (13) shows that, in the case of the proton (deuteron) transfer reactions (3a) and (3b), there is very little laboratory kinetic energy release, i.e., the product ions essentially maintain the velocity of the neutral target molecule. Table V compares the measured ion energies of the first band peaks with those obtained using Eq. (13). The table also includes the calculated internal energies, assuming an exothermicity of 1.12 eV (Ref. 33) and using the measured product ion laboratory energies. Assuming a stationary target, the internal energy $E_{\rm int}$, of the product ions is obtained from

$$E_{\rm int} = E_{\rm c.m.} - E_{\rm th} - E_{\rm kin}, \tag{14}$$

where $E_{\rm th}$ is the thermodynamic threshold for the particular reaction and $E_{\rm kin}$ is the total kinetic energy release. Assuming zero-degree scattering, $E_{\rm kin}$ is obtained from the center-of-mass velocity $u_{\rm sec}$ of the secondary ion:

$$E_{\rm kin} = [(m_1 + m_2)/m_4] \cdot (m_3/2) u_{\rm sec}^2, \tag{15}$$

where m_4 is the neutral product mass, and where

$$u_{\rm sec}^2 = (v_{\rm c.m} - v_{\rm sec})^2. \tag{16}$$

With the exception of some of the high collision energy measurements, which suffer from small product signal levels, the experimental data agrees well with the predictions of the model. As anticipated from Eq. (13), the secondary ion energies of the deuteron transfer exceed those of the proton transfer and more noticeably increase with collision energy. The internal energies lie substantially below the dissociation limits of H_3O^+ which are reported to be 7.18 ± 0.08 eV (Ref. 34) and 6.2 eV (Ref. 33) for the dissociation products $H^+ + H_2O$ and $H + H_2O^+$, respectively.

The model can be tested further by examining the isotope effect. According to the spectator stripping model, no isotope effect is observed when basing the isotopic comparison on pseudo collision energies $E'_{\rm c.m.}$ involving only the acceptor and the transferred particle. Consequently, if the reaction cross section has an observable collision energy dependence within the energy range of interest, an isotope effect should be observed when plotting the data on a conventional collision energy scale, as in Fig. 5. The measured cross sections are plotted versus the pseudo center-of-mass collision energies $E'_{\rm c.m.}$ in Fig. 11. The energy $E'_{\rm c.m.}$ is calculated from

$$E'_{\rm c.m.} = (m_T m_2/m_1 m_3) \cdot E_{\rm prim}. \tag{17}$$

At energies above $E'_{\rm c.m.} = 0.4$ eV (4.4 eV c.m.), an isotope effect is no longer apparent, supporting the spectator stripping model. Below 0.4 eV, the deuteron transfer cross section becomes substantially greater than that of proton transfer. The model clearly no longer applies here. At these low energies the collision complex lifetime becomes comparable with the rotational period of the complex. It is conceivable therefore that we are observing a transition from direct to statistical collision dynamics. A change in dynamics is also reflected at a relative energy of 1.3 eV in reaction (3b), where a product ion energy substantially higher than predicted by Eq. (13) is observed. Crossed beam experiments by Herman[35] show that at a relative energy of 1.34 eV, a substantial fraction of oxonium ions are produced via a long-lived complex.

From the good agreement with the predictions of the spectator stripping model, we conclude that the proton transfer channel leading to the near-thermal energy ions represents collisions at relatively large impact parameters, in which little scattering from the repulsive part of the intermolecular potential occurs. On the other hand, both the second and third bands are most likely produced by small impact

TABLE V. Comparison of the first band laboratory energies $E_{\rm sec}$ (expt) of reactions (3a) and (3b) with those predicted using a spectator stripping model $E_{\rm sec}$ (calc) [Eq. (13)]. The internal energies $E_{\rm int}$ obtained from Eqs. (14)–(16) for the measured secondary ion energies are also listed.

$E_{\rm prim}$ (eV)	$E_{\rm sec}$ (expt) (eV)	$E_{\rm sec}$ (calc) (eV)	$E_{\rm int}$ (calc) (eV)
$H_2O^+ + D_2{}^{18}O \rightarrow OH + HD_2{}^{18}O^+$ (3a)			
5.1	0.04 ± 0.05	0.01	1.8
9.5	0.06 ± 0.07	0.02	2.2
14.3	0.13 ± 0.07	0.04	3.2
19.0	0.10 ± 0.05	0.05	3.1
29.1	0.08 ± 0.05	0.07	2.9
36.4	0.07 ± 0.07	0.09	2.6
43.8	0.15 ± 0.07	0.11	4.3
$D_2O^+ + D_2{}^{18}O \rightarrow OD + D_3{}^{18}O^+$ (3b)			
2.5	0.23 ± 0.10	0.02	2.1
4.1	0.07 ± 0.07	0.03	1.8
9.0	0.12 ± 0.05	0.08	2.4
14.0	0.13 ± 0.07	0.12	2.6
19.2	0.18 ± 0.08	0.16	3.1
24.1	0.19 ± 0.10	0.20	3.2
29.1	0.21 ± 0.10	0.24	3.4
34.1	0.09 ± 0.15	0.28	1.4
39.4	0.17 ± 0.15	0.33	2.7

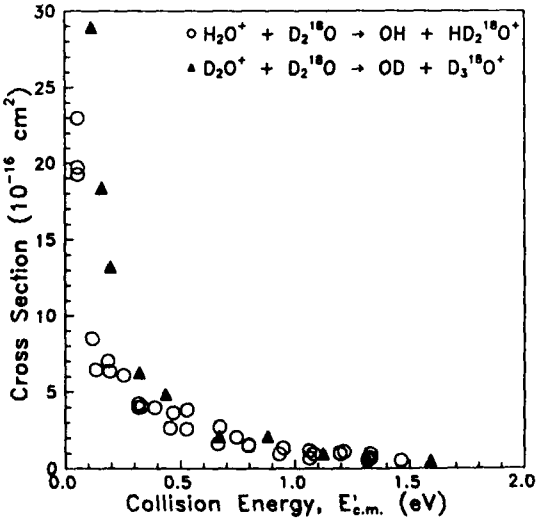

FIG. 11. Spectator stripping energy dependence of cross sections for proton and deuteron transfer. The spectator stripping energy $E'_{c.m}$ is the relative energy obtained when the collision is regarded as occurring between a proton and a water molecule.

parameter collisions. Such collisions transfer translational energy into internal energy more efficiently and are also accompanied by large-angle scattering. Table VI lists the internal energies calculated for the second and third TOF band centers of reaction (3a) and (3b) using the observed laboratory energies. Assuming that the product ions comprising the second band are not due to large-angle scattering in the laboratory frame, it is seen that these ions are associated with collisions where the reaction energy appears to be almost entirely channeled into internal excitation of the products. At higher collision energies a large fraction of this energy must be channeled into the neutral hydroxyl product in order to produce a nondissociative oxonium ion. The hydroxyl radical can therefore be excited beyond its dissociation threshold. The reaction

$$H_2O^+ + H_2O \rightarrow H_3O^+ + O + H \qquad (18)$$

has a threshold of only 3.23 eV.[33] In order to calculate the internal energy for this process, Eq. (15) must include both neutral products. The small center-of-mass kinetic energy release observed in the second band product ions can then no longer be associated with high internal excitation, since a major fraction of the total product translational energy is expected to be partitioned to the light hydrogen atom due to conservation of linear momentum and energy. In addition, it is necessary to know whether the three products of reaction (18) are produced simultaneously or via a dissociative hydroxyl radical. The fact that the second band ions of reaction (3a) are observed to be slightly forward scattered may indicate that the second band ions are produced through reaction (18) via a sequential mechanism.

The ion products of the very weak forward-scatterd third band are associated with higher internal energies than calculated for the first band. They are presumably produced in head-on collisions, causing 180° scattering of the neutral spectator. This is consistent with the higher internal excitation observed in small impact parameter collisions compared with grazing, large impact parameter collisions such as those leading to the near-thermal ions.[36] From the measured statistical weights, we estimate the cross section for the second and third band ions to be less than 5×10^{-18} and 10^{-18} cm^2, respectively.

Our measured total cross sections for reaction (1), which are essentially the proton transfer cross sections, are approximately a factor of 2 higher than the cross sections reported by Turner and Rutherford.[13] These authors used a crossed beam apparatus which involved calibrating the neutral target density and collection efficiency. Their study of reaction (1) included neither isotopic analysis nor product kinetic energy analysis. The authors did, however, address the two possible direct transfer channels and their different product velocity distributions. Not knowing the branching ratios of the two processes, they chose a collection efficiency halfway between unity for the atom pickup case and their determined charge exchange collection efficiency related to the proton transfer reaction in order to report an integral cross section for reaction (1). Since our measurements show that the oxonium ions are primarily produced through proton transfer and that they have a largely isotropic velocity distribution, we conclude that the authors of Ref. 13 assumed a collection efficiency that was too high, resulting in their reported cross sections being too low.

TABLE VI. Internal energies E_{int} calculated for the second and third TOF band center ions of the proton (deuteron) transfer reactions (3a) and (3b) using the ion product laboratory translational energies listed in Table II. The high second band internal energies indicate that these oxonium ions are associated with the simultaneous production of an oxygen atom and a hydrogen atom [reaction (18)].

$E_{c.m.}$ (eV)	E_{int} 2nd band (eV)	E_{int} 3rd band (eV)
$H_2O^+ + D_2{}^{18}O \rightarrow OH + HD_2{}^{18}O^+$ (3a)		
2.81	···	···
5.23	···	4.2
7.87	···	7.0
10.5	11.2	5.7
16.1	16.8	···
20.0	20.5	5.4
24.1	24.7	···
$D_2O^+ + D_2{}^{18}O \rightarrow OD + D_3{}^{18}O^+$ (3b)		
2.25	···	···
4.71	···	3.4
7.33	···	5.5
10.1	11.2	4.2
12.6	13.7	7.0
15.2	16.3	7.5
17.9	19.0	···
20.6	20.9	···

B. Charge exchange channel

To our knowledge, no work is reported in the literature on the symmetric charge exchange reaction. Our cross-section measurements show that charge exchange is clearly the most efficient channel of H_2O^+–H_2O collisions at collision energies above 1 eV. The magnitude of the charge exchange cross sections are approximately half the values obtained for charge exchange of N_2^+ and O^+ with water.[17,37] The most striking difference between the latter charge exchange examples and the one studied here is the prominent TOF band observed at high laboratory energies (second TOF band). From the statistical weights listed in Table III, we estimate the cross sections for the second band ions to be less than 10^{-17} cm^2.

The second TOF band ions can be either due to high internal excitation of the collision products or due to the dissociation of oxonium ions produced in the proton transfer reaction with internal energy exceeding the dissociation threshold. If the latter possibility is occurring, the H_2DO^+ intermediate [in the case of reaction (4b)] would dissociate to either H_2O^+ or HDO^+, assuming that the excess energy is distributed among the O–H(D) bonds prior to dissociation. Since considerable mass 19 signal in reaction (4b) stems from charge transfer to HDO target gas impurities, the TOF spectra for mass 18 and 19 ions need to be compared to verify the existence of dissociation products in the charge exchange channel measurements. Table VII lists the

TABLE VII. Normalized weights of second band of reaction (4b) TOF spectra obtained for mass 18 and 19 ions.

$D_2{}^{18}O^+ + H_2O \rightarrow D_2{}^{18}O + H_2O^+$ (4b)		
$E_{c.m.}$ (eV)	mass 18 (%)	mass 19 (%)
3.96	0.6	0.7
8.64	1.7	2.1
12.7	2.6	5.8
17.1	2.2	6.4
21.7	6.6	16.1

normalized weights of the second band observed in the mass 18 and mass 19 TOF spectra. At 3.96 eV, there is no notable difference between the mass 18 and mass 19 TOF spectra and therefore the HDO^+ ions stem from impurities and cannot be attributed to the dissociation of oxonium ions. This is not surprising, since the collision energy is less than the required energy for dissociation of 6.2 eV.[33]

At collision energies above about 8.0 eV, the ratio between the mass 19 and mass 18 second band normalized weights increases dramatically with collision energy. We attribute this increase to HDO^+ ions which are produced through dissociative decay of H_2DO^+ proton transfer products. The second band ions therefore at least partly originate from dissociating oxonium ions.

Table VIII lists the internal energies for reactions (4a) and (4b) calculated using the determined laboratory energies of the second band ions and assuming that the product ions are formed through charge exchange rather than via proton transfer. It is seen that at collision energies between 10 and 20 eV, large proportion of the reaction energy appears to be converted into internal energy of the products. At higher energies, the products observed in the second TOF band are scattered slightly forward with respect to the center-of-mass velocity and the collision energy is converted less efficiently.

TABLE VIII. Internal energies E_{int} calculated from the second band TOF band centers of the reactions (4a) and (4b) charge transfer products.

$H_2O^+ + D_2{}^{18}O \rightarrow H_2O + D_2{}^{18}O^+$ (4a)	
$E_{c.m.}$ (eV)	E_{int} (2^{nd} band) (eV)
2.81	...
6.05	...
10.6	10.6
16.1	14.8
21.8	19.0
27.1	19.0
$D_2{}^{18}O^+ + H_2O \rightarrow D_2{}^{18}O + H_2O^+$ (4b)	
3.96	2.9
8.64	7.9
12.7	12.3
17.1	15.3
21.7	19.0

The internal energies listed in Table VIII do not apply if the second band ions are assumed to stem entirely from dissociating oxonium ions. In this case very little center-of-mass kinetic energy is expected to appear in the heavy ionic product, since almost all of the kinetic energy would be partitioned to the hydrogen atom due to conservation of momentum and energy. The center-of-mass kinetic energy observed in the water ion products at higher collision energies is therefore related to the kinetic energy partitioned to the oxonium ion prior to dissociation. Since it is not known how the excess energy is distributed among the three O–H(D) bonds prior to dissociation of the oxonium ion, the comparison between the mass 18 and mass 19 second band signals in reaction (4b) is insufficient to determine the proportion of the second band signal that is due to the dissociation product.

C. OH^+ production

The measured kinetic energy release from reaction (5) exceeds the total available excess energy, indicating that the ion product can only be formed from excited primary ions. We believe that small amounts of metastable ions with large collision-induced dissociation cross sections are producing the observed OH^+ (OD^+) signals. The observed cross sections in Fig. 9 are not representative of the actual collision-induced dissociation cross section since the fraction of metastable ions in the primary beam is unknown. The highly forward peaked ion signals indicate that the dissociation process occurs at large impact parameters, which would result in a large cross section if the dissociation probability is high. A loosely bound primary ion, excited to levels close to the dissociation threshold, would account for large collision-induced dissociation cross sections.

V. CONCLUSION

The ion–molecule reaction between H_2O^+ and H_2O at suprathermal energies yields two main products, H_3O^+ and the symmetric charge exchange product. At collision energies above 1 eV, charge exchange is the most efficient reaction, where a cross section between 6 and 10×10^{-16} cm^2 is measured. The oxonium ions are mainly produced through transfer of a proton from the primary ion to the target molecule. The cross section for oxonium ion production through primary ion hydrogen atom pickup is at least an order of magnitude smaller than the proton transfer cross section throughout the measured energy range.

Both charge exchange and proton transfer primarily yield near-thermal product ions in the laboratory frame, whereas the significantly weaker atom-pickup channel produces strongly forward-peaked product ions. These product laboratory energies are characteristic of large impact parameter collisions involving a direct reaction mechanism. The measured laboratory energies of both atom-pickup and proton transfer channels are in good agreement with those predicted by the spectator stripping model.[26–31] The observed proton transfer channel isotope effect is in agreement with the predictions of this model at collision energies above 4 eV. At lower collision energies the model fails to account for the

isotope effect, indicating a transition to statistical dynamics involving an intermediate complex.

Production of high laboratory ion energies are observed in both charge exchange and proton transfer channels. At collision energies above $E_{c.m.} = 10$ eV, a significant fraction of the high energy water ions detected in the charge exchange channel are found to be the products of dissociating oxonium ions. The production of the high energy ions observed in the proton transfer channel is suggested to be accompanied by the dissociation of the neutral product hydroxyl radical. We estimate the cross sections for forming the excited products to be less than 10^{-17} cm^2.

ACKNOWLEDGMENTS

One of us (CRL) is grateful to the Air Force Office of Scientific Research (AFSC, USAF) for sponsoring research under contrast F49620-88-C0053. We thank Z. Herman for communicating his results prior to publication.

[1] M. M. Mann, A. Hustrulid, and J. T. Tate, Phys. Rev. **58**, 340 (1940).
[2] R. A. Fluegge, J. Chem. Phys. **50**, 4373 (1969).
[3] A. Good, D. A. Durden, and P. Kebarle, J. Chem. Phys. **52**, 212 (1970).
[4] R. C. Bolden and N. D. Twiddy, Faraday Disc. Chem. Soc. **53**, 192 (1972).
[5] W. T. Huntress and R. F. Pinizzotto, J. Chem. Phys. **59**, 4742 (1973).
[6] J. Sunner and I. Szabo, Int. J. Mass Spect. Ion Phys. **31**, 213 (1979).
[7] R. Narcisi, E. Trzsinski, G. Frederico, L. Wlodyka, and D. Delorey, in AIAA Shuttle Environment and Operations II Conference Proceedings (1983), p. 183.
[8] J. M. Grebowsky, H. A. Taylor, Jr., and M. W. Pharo, III, Planet. Space Sci. **35**, 501 (1987).
[9] E. Wulf and U. von Zahn, J. Geophys. Res. **91**, 3270 (1986).
[10] K. W. Ogilvie, M. A. Coplan, P. Bochsler, and J. Geiss, Science **232**, 374 (1986).
[11] H. Balsiger, K. Altwegg, F. Buehler, J. Geiss, A. G. Ghielmetti, B. Goldstein, R. Goldstein, W. T. Huntress, W.-H. Ip, A. J. Lazarus, A. Meier, M. Neugebauer, U. Rettenmund, H. Rosenbauer, R. Schwenn, R. D. Sharp, E. G. Shelley, E. Ungstrup, and D. T. Young, Nature **321**, 330 (1986).
[12] E. Murad, Planet. Space Sci. **33**, 421 (1985).
[13] B. R. Turner and J. A. Rutherford, J. Geophys. Res. **73**, 6751 (1968).
[14] K. R. Ryan, J. Chem. Phys. **52**, 6009 (1970).
[16] W. B. Maier and E. Murad, J. Chem. Phys. **55**, 2307 (1971).
[17] R. A. Dressler, J. A. Gardner, R. H. Salter, F. J. Wodarczyk, and E. Murad, J. Chem. Phys. **92**, 1117 (1990).
[18] J. A. Gardner, R. A. Dressler, R. H. Salter, and E. Murad, Geophysics Laboratory Technical Report, GL-TR-89-0344 (1989).
[19] E. Lindemann, R. W. Rozett, and W. S. Koski, J. Chem. Phys. **56** 5490 (1972).
[20] L. Karlson, L. Mattsson, R. Jadrny, R. G. Albridge, S. Pinchas, T. Bergmark, and K. Seigbahn, J. Chem. Phys. **62**, 4745 (1975).
[21] F. T. Chau, J. Elect. Spect. Ref. Phen. **48**, 389 (1989).
[22] P. Erman and J. Brzozowski, Phys. Lett. A **46**, 79 (1973).
[23] M. Tsuji, J. P. Maier, H. Obase, and Y. Nishimura, Chem. Phys. Lett. **147**, 619 (1988).
[24] H. Lew, Can. J. Phys. **54**, 2028 (1976).
[25] Secondary ion TOF bands are referred to numerically (first, second, third) in increasing secondary ion energy.
[26] Z. Herman, J. Kerstetter, T. Rose, and R. Wolfgang, Disc. Faraday Soc. **44**, 123 (1967).
[27] W. R. Gentry, E. A. Gislason, Y. T. Lee, B. H. Mahan, and C. W. Tsao, Disc. Farad. Soc. **44**, 137 (1967).
[28] A. Henglein, in Proceedings of the International School of Physics "Enrico Fermi", C. XLIV, Mol. Beams and Kinetics, edited by Ch. Schlier (Academic, New York, 1970).
[29] K. Lacmann and A. Henglein, Ber. Bunsenges. Phys. Chem. **69**, 292 (1965).
[30] A. Ding, K. Lacmann, and A. Henglein, Ber. Berl. Buns. Ges. **71**, 596 (1967).
[31] A. Henglein, Adv. Mass Spectrom. **3**, 331 (1966).
[32] S. Tomoda and K. Kimura, Chem. Phys. **82**, 215 (1983).
[33] S. G. Lias, J. E. Bartmess, J. F. Liebman, J. L. Holmes, R. D. Levin, and W. G. Mallard, J. Phys. Chem. Ref. Data **17**, Supp. 1 (1988).
[34] C. Y. Ng, D. J. Trevor, P. W. Tiedemann, S. T. Ceyer, P. L. Kronebusch, B. H. Mahan, and Y. T. Lee, J. Chem. Phys. **67**, 4235 (1977).
[35] Z. Herman (private communication).
[36] B. H. Mahan, Acc. Chem. Res. **3**, 393 (1970).
[37] M. Heninger, S. Fenistein, G. Mauclaire, R. Marx, and E. Murad, Geophys. Res. Lett. **16**, 139 (1989).